0D/2D P-doped $Zn_xCd_{1-x}S$/g-C_3N_4 Heterojunctions towards Highly Efficient Photocatalytic Hydrogen Evolution

Hongfei Yin, Xiaoheng Liu[*]

Key Laboratory of Education Ministry for Soft Chemistry and Functional Materials,
Nanjing University of Science and Technology, Nanjing, China

Abstract

Solar-driven water splitting over semiconductor photocatalysts is a promising approach for converting solar energy into renewable and storable chemical energy. CdS, an efficient photocatalyst for hydrogen evolution, suffers from high recombination of photogenerated electron-hole pairs and high photocorrosion in aqueous media, which limit its practical applications. Doping and the formation of heterojunctions are two efficient methods to improve the photocatalytic activities of photocatalysts. Herein, we rationally designed and fabricated P-doped 0D/2D $Zn_xCd_{1-x}S$/g-C_3N_4 nanocomposites by in-situ immobilizing $Zn_xCd_{1-x}S$ onto the surface of g-C_3N_4 nanosheets in a hydrothermal environment, followed by a phosphorization process. The as-prepared P-doped $Zn_xCd_{1-x}S$/g-C_3N_4 nanocomposites were systematically characterized by analyzing the phase structure, chemical components, electronic and optical properties and separation of charge carriers. More importantly, these P-doped $Zn_xCd_{1-x}S$/g-C_3N_4 heterostructures have been proven to be highly efficient visible light responsive photocatalysts for hydrogen evolution, and meanwhile exhibit excellent photo-stability during recycling runs. The sufficient evidence exhibit that the significantly improved photocatalytic performance is mainly attributed to the prolonged lifetime of charge carriers and the improved separation efficiency of photogenerated electron-hole pairs.

Keywords: P-doped $Zn_xCd_{1-x}S$/g-C_3N_4, heterojunctions, photocatalysis, hydrogen evolution

1. Introduction

Since the discovery of photocatalytic water splitting on TiO_2 electrodes by Fujishima and Honda in 1972, the utilization of solar energy for the alleviation of steadily worsening environmental issues and energy crisis has attracted a lot of research interests, and a large number of photocatalytic materials, including metal oxide, metal sulfide, organic compounds, and composites, have been developed for various applications such as water splitting, CO_2 reduction, wastewater treatment and nitrogen fixation [1-5]. However, pure TiO_2 demonstrated extremely low photocatalytic activity due to its relatively large band gap (3.2 eV for the anatase phase and 3.0 eV for the rutile phase). The limited UV-responsive activity of TiO_2 largely inhibits its large scale application because UV light makes up just a small part of the total solar spectrum reaching the earth surface. As in so doing, to explore and design visible light driven photocatalysts is very important to improve the photocatalytic efficiency towards practical applications [6–8].

Recently, much research has been focused on the development of visible-light-responsive photocatalysts to take advantage of the solar light resources more effectively because visible light constitutes a larger proportion than UV light in solar light. In fact, metal chalcogenides due to appropriate band gap width and band edge position have elicited more and more

* Corresponding author. E-mail address: xhliu@njust.edu.cn
Tel.: +025-84315943; Fax: +025-84315943

attention in photocatalytic H_2 evolution [9]. Especially, CdS with suitable band edge positions and appropriate band gap of 2.4 eV has been proven to be an efficient semiconductor H_2-production photocatalyst and has been extensively studied [10]. However, there are several obvious problems that restrict the wide application of CdS to a large extent. In detail, quick recombination of photogenerated charge carriers and instability during the photocatalytic reaction owing to photocorrosion, where S^{2-} in CdS can be oxidized by photogenerated holes accompanied by the release of Cd^{2+} [11]. These drawbacks can be overcome by elemental doping into CdS lattices, such as Ni, Mn, Zn and P [12-15], and constructing type-II semiconductor heterostructures [16-19], due to its effectiveness for spatially separating the photogenerated electron-hole pairs through the band alignment between two semiconductors [20, 21].

$Zn_xCd_{1-x}S$ solid solution, as a hydrogen-producing photocatalyst with superior performance, has been extensively studied due to its tunable band structure, which makes it possible to balance the redox ability of photo-induced charge carries and absorption of visible light. To date, $Zn_xCd_{1-x}S$ solid solution is the most efficient sulfide photocatalyst for hydrogen production without any co-catalyst [22, 23]. Unfortunately, the catalytic activity of $Zn_xCd_{1-x}S$ solid solution is still limited due to the high recombination rate of electron-hole pairs. Metal-free polymeric graphitic carbon-nitrogen(g-C_3N_4) with suitable band edge positions and appropriate band gap has emerged as appealing visible light driven photocatalyst and widely applied in the field of photocatalysis due to its simple syntheses, nontoxicity, earth-abundant, and excellent structural stability in the thermal and chemical environment [16, 17]. However, the low specific surface area and high recombination rate of photogenerated electron-hole pairs originate from the bulk structure and the presence of internal grain boundary, lead to the low photocatalytic activity, largely limiting the practical application of bulk g-C_3N_4 [24, 25]. Based on the band structure of $Zn_xCd_{1-x}S$ and g-C_3N_4, Guo et al. combined g-C_3N_4 and $Cd_xZn_{1-x}S$ to construct heterojunctions by hydrothermal method, the activity of the composite is 1.95 times than that of pure $Cd_{0.5}Zn_{0.5}S$ [26]. Jin et al. reported that water splitting performance of the binary $Cd_{0.2}Zn_{0.8}S$/g-C_3N_4 composite photocatalyst is about 1.5 times higher than pure $Cd_{0.2}Zn_{0.8}S$ [27].

In the present work, we rationally designed and fabricated P-doped 0D/2D $Zn_xCd_{1-x}S$/g-C_3N_4 nanocomposites by in-situ immobilizing $Zn_xCd_{1-x}S$ onto the surface of g-C_3N_4 nanosheets in a hydrothermal environment, followed by a phosphorization process. We anticipate that g-C_3N_4 could act as substrates to develop a suitable heterogeneous interface to promote photo-induced interfacial charge transfer. The as-fabricated P-doped $Zn_xCd_{1-x}S$/g-C_3N_4 nanocomposites and the enhancement of photocatalytic activities were systematically characterized by XRD, FESEM, TEM, and electrochemical measurements.

2. Experimental

Melamine ($C_6H_6N_6$), zinc acetate dehydrates ($Zn(Ac)_2 \cdot 2H_2O$), cadmium acetate dehydrates ($Cd(Ac)_2 \cdot 2H_2O$) and Thioacetamide (TAA) were bought from Sinopharm Chemical Reagent Co., Ltd. (Shanghai, China). $NaH_2PO_2 \cdot H_2O$ was bought from Macklin (Shanghai, China). All reagents were of analytic purity, used without any purification.

2.1. Preparation of bulk g-C_3N_4

Melamine powder was put into an alumina crucible with a cover and heated to 550 ℃ at a heating rate of 2.3 ℃/ min and maintained at this temperature for 4h. The resulted yellow product was collected and ground into powder for further use.

2.2. Preparation of g-C_3N_4 nanosheets

The as-prepared bulk g-C_3N_4 (1g) was mixed with 10 mL of H_2SO_4 and stirred overnight at room temperature. Then the mixture was slowly poured into 150 mL of deionized water and sonicated for exfoliation. The obtained suspension was centrifuged, washed thoroughly with deionized water to remove the residual acid, and finally dried at 80 ℃ in air overnight.

2.3. Preparation of $Zn_{0.5}Cd_{0.5}S$/g-C_3N_4

50 mg g-C_3N_4 nanosheets were dispersed completely into a mixed solvent consisting of 50 mL of deionized water by ultrasonication, then 1mmol zinc acetate dihydrate ($Zn(Ac)_2 \cdot 2H_2O$), and 1mmol cadmium acetate dihydrate ($Cd(Ac)_2 \cdot 2H_2O$)

were dissolved into the above suspension, the mixture was stirred magnetically for 2 hours. Subsequently, NaOH aqueous solution was added dropwise followed by the addition of 2mmol thioacetamide(TAA), then stirring for 4h at room temperature. Then the mixture was transferred to a 100 mL polytetrafluoroethylene-lined stainless autoclave at 180 ℃ for 12 h under autogenous pressure in an electric oven. After cooling down to room temperature naturally, the product was collected, washed by water and ethanol for several times, and fully dried at 60 ℃ to obtain the final $Zn_{0.5}Cd_{0.5}S/g-C_3N_4$ nanocomposites, denoted as GS. The pure $Zn_{0.5}Cd_{0.5}S$ was prepared with the same method in the absence of $g-C_3N_4$.

2.4. Preparation of P-doped $Zn_xCd_{1-x}S/g-C_3N_4$

The P-doped $Zn_{0.5}Cd_{0.5}S/g-C_3N_4$ sample was synthesized using sodium hypophosphite $(NaH_2PO_2 \cdot H_2O)$ as the P precursor. Typically, $Zn_{0.5}Cd_{0.5}S/g-C_3N_4$ and $NaH_2PO_2 \cdot H_2O$ were mixed together and finely grind with a mortar. Then, the mixture was heated at 300 ℃ in an N_2 atmosphere (a ramp rate of 2 ℃/min). After cooling down to room temperature naturally, the product was collected, washed by water and ethanol several times, and fully dried at 60 ℃ overnight, and the samples were denoted as PGS.

2.5. Catalysts characterization

The crystal structures and phase states of the photocatalysts were analyzed by X-ray diffractometry using a Bruker D8 Advance diffractometer with Cu Kα radiation(λ= 0.15418 nm) at an operating voltage of 40kV and an operating current of 40mA. The morphologies of the samples were observed by field-emission scanning electron microscope (FESEM, Hitachi S-4800) with an acceleration voltage of 15.0kV and transmission electron microscope (TEM, JEOL JEM-2100) at an acceleration voltage of 200kV. UV–vis diffused reflectance spectra were recorded on an Evolution 220 UV-vis spectrophotometer (Thermo Fisher, America) from 200 to 800nm.

2.6. Electrochemical measurements

Electrochemical Impedance Spectroscopy (EIS) and photocurrent measurements were performed in a conventional three-electrode on a CHI-760E electrochemical workstation. Ag/AgCl and platinum wire were used as the reference electrode and counter electrode, respectively. A 0.5 M Na_2SO_4 aqueous solution was used as the electrolyte. A 300W Xe lamp equipped with a 420nm cut-off filter was employed as a light source. The working electrode was prepared as follow: 4 mg of the as-obtained sample and 10μL Nafion solution (5 wt%) were dispersed in 1 mL water-ethanol solution with a volume ratio of 3:1 by sonicating for 1 h to form a homogeneous slurry. Then 100μ L of the dispersion was loaded onto a 1cm×3cm ITO-coated glass substrate with a coating area of 1cm^2.

2.7. Catalysts activity evaluations

The photocatalytic activities of as-fabricated P-doped $Zn_{0.5}Cd_{0.5}S/g-C_3N_4$ nanocomposites were estimated by the degradation of Rhodamine B (RhB) dye and hydrogen evolution from water splitting with the exposure of visible light irradiation. A 300 W xenon lamp equipped with a cut-off filter of 420 nm was employed as the light source for the photocatalytic reaction. During the photodegradation reaction, 20 mg of photocatalysts was totally dispersed into 50 mL aqueous solution of RhB dye with an initial concentration of 10 mg/L. Prior to irradiation, the suspension was drastically stirred in the dark for 1 h to achieve adsorption-desorption equilibrium between the photocatalysts and RhB. At an interval of 10 min, 3 mL aliquots were collected, centrifuged, and then analyzed by recording variations at the wavelength of maximal absorption (λ= 554 nm) on a UV-vis spectrometer (UV-1201). As for hydrogen generation, 50 mg of the prepared $Zn_{0.5}Cd_{0.5}S$, GS and PGS were used for measuring the hydrogen evolution from 200 ml 0.35 M Na_2S and 0.25 M Na_2SO_3 aqueous solution under visible light irradiation. For $g-C_3N_4$, 50mg sample was dispersed into 200 ml aqueous solution containing triethanolamine (10 vol%) as a sacrificial electron donor. The photocatalytic system for hydrogen evolution (PLX-10A) was evacuated several times to remove the air inside the reaction system prior to irradiation. The evolved hydrogen was analyzed by on-line gas chromatography (GC-1690, Jiedao, TCD, Ar carrier).

3. Results and Discussion

The typical XRD patterns of g-C_3N_4 bulk, g-C_3N_4 nanosheets, $Zn_{0.5}Cd_{0.5}S$/g-C_3N_4, and P-doped $Zn_{0.5}Cd_{0.5}S$/g-C_3N_4 nanocomposites were illustrated in Fig. 1(a) and (b). The g-C_3N_4-bulk exhibit two obvious characteristic diffraction peaks located at 13.1° and 27.4°, which could be ascribed to (100) and (002) diffraction plane of graphitic carbon nitrogen, separately representing the in-plane structural packing motif and inter-planar stacking peak of aromatic systems [28]. It is found that the (002) diffraction at around 27.4°relating to the characteristic interlayer stacking structure is shifted to 27.9°, indicating that the bulk g-C_3N_4 was exfoliated into nanosheet. The XRD patterns of $Zn_{0.5}Cd_{0.5}S$/g-C_3N_4 and P-doped $Zn_{0.5}Cd_{0.5}S$/g-C_3N_4 nanocomposites display similar characteristic diffraction peaks, it is noticeable that the main three diffraction peaks of P-doped $Zn_{0.5}Cd_{0.5}S$ in the range of 24.5-30°slightly shift to smaller diffraction angles after P doping, implying the appearance of lattice expansion after P doping.

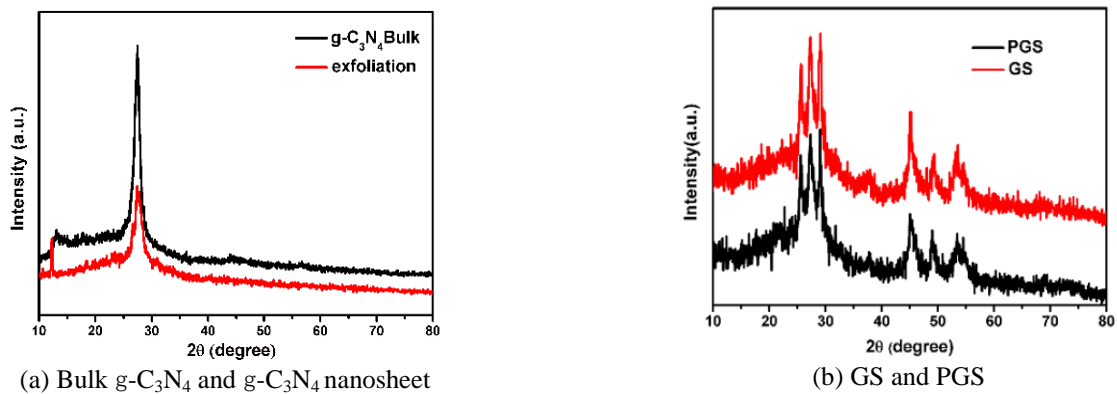| (a) Bulk g-C_3N_4 and g-C_3N_4 nanosheet	(b) GS and PGS

Fig. 1 XRD patterns of the as-prepared samples

The in-situ growth strategy for preparing the composite is schematically illustrated in Fig.2. A previous electrophoresis experiment illustrated that g-C_3N_4 is negatively charged when it is dispersed in water because of the deprotonation of amine groups on the g-C_3N_4 surface [29]. When Cd(Ac)$_2$ and Zn(Ac)$_2$ are introduced into the suspension, Zn^{2+} and Cd^{2+} can be tightly adsorbed onto the g-C_3N_4 nanosheets through electrostatic interaction. Upon the addition of NaOH and TAA, Zn^{2+} and Cd^{2+} react with S^{2-} to generate $Zn_{0.5}Cd_{0.5}S$ NPs. As a result, the $Zn_{0.5}Cd_{0.5}S$ particles are well deposited on g-C_3N_4 nanosheets, and a $Zn_{0.5}Cd_{0.5}S$/g-C_3N_4 composite is obtained. The P-doped $Zn_{0.5}Cd_{0.5}S$/g-C_3N_4 nanocomposites can be obtained by the phosphorization of $Zn_{0.5}Cd_{0.5}S$/g-C_3N_4 using NaH_2PO_2 as P source.
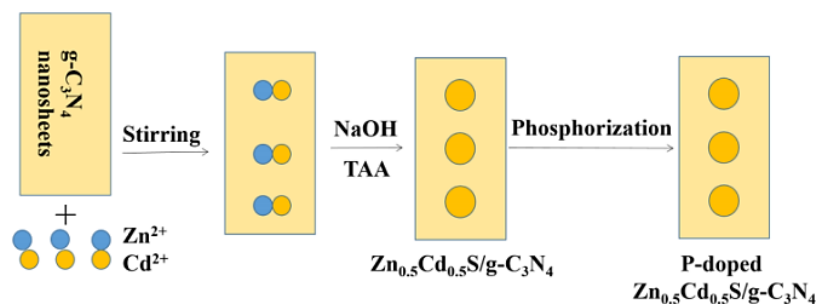

Fig. 2 Schematic of the in-situ fabrication of the P doped $Zn_{0.5}Cd_{0.5}S$/g-C_3N_4 composite

The morphology of the as-prepared samples was investigated by SEM and TEM as shown in Fig. 3. Fig. 3(b) is a typical TEM image of pure $Zn_{0.5}Cd_{0.5}S$ nanoparticles with a size of about 20nm. Fig. 3(c) shows the TEM pattern of $Zn_{0.5}Cd_{0.5}S$/g-C_3N_4, which exhibits a 0D/2D nanostructure and g-C_3N_4 with length and width of 400nm and 800nm, respectively. Fig. 3(a) and Fig. 3(d) are SEM and TEM images of P-doped $Zn_{0.5}Cd_{0.5}S$/g-C_3N_4, respectively. A fluffy structure can be clearly observed. These features could provide an appropriate location for developing 0D/2D heterostructure, similar to $Zn_{0.5}Cd_{0.5}S$/g-C_3N_4, indicating that the doping of P didn't change the morphology of the original $Zn_{0.5}Cd_{0.5}S$/g-C_3N_4.
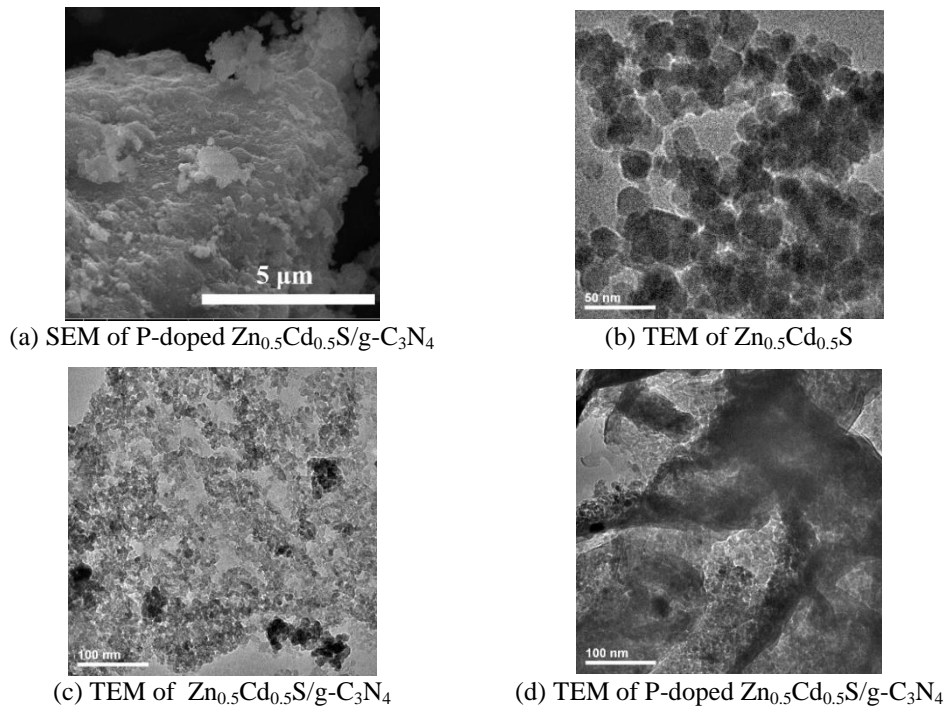
(a) SEM of P-doped $Zn_{0.5}Cd_{0.5}S$/g-C_3N_4

(b) TEM of $Zn_{0.5}Cd_{0.5}S$

(c) TEM of $Zn_{0.5}Cd_{0.5}S$/g-C_3N_4

(d) TEM of P-doped $Zn_{0.5}Cd_{0.5}S$/g-C_3N_4

Fig. 3 Morphology of the as-prepared samples

The optical properties of as-obtained $Zn_{0.5}Cd_{0.5}S$, g-C_3N_4 nanosheets, $Zn_{0.5}Cd_{0.5}S$/g-C_3N_4 as well as P-doped $Zn_{0.5}Cd_{0.5}S$/g-C_3N_4 nanocomposites were characterized by UV-vis diffuse reflectance spectra (UV-vis DRS) and displayed in Fig. 4. It is clearly seen that pure $Zn_{0.5}Cd_{0.5}S$ possess strong ability towards light absorption from the UV range to the visible light region up to 531 nm, while the absorption threshold of pure g-C_3N_4 nanosheets is only about 422 nm. The introduction of g-C_3N_4 nanosheets has an obvious effect on the optical property of $Zn_{0.5}Cd_{0.5}S$. Remarkably, the obtained binary catalyst shows a small absorption blue-shift as a comparison to pure $Zn_{0.5}Cd_{0.5}S$. Such result may be ascribed to the interaction between the $Zn_{0.5}Cd_{0.5}S$ and g-C_3N_4 nanosheets and improved light scattering resulted from the smaller particle sizes of $Zn_{0.5}Cd_{0.5}S$ in $Zn_{0.5}Cd_{0.5}S$/g-C_3N_4 nanocomposites [30]. After the doping of P, the absorption edge almost shifts to 680nm, the possible reason is that the heterojunction formed between $Zn_{0.5}Cd_{0.5}S$ and g-C_3N_4 nanosheets may effectively decrease contact barrier and strengthen electronic coupling of the semiconductors, thus resulting in the enhanced visible light absorption, leading to the enhancement of photocatalytic activities.
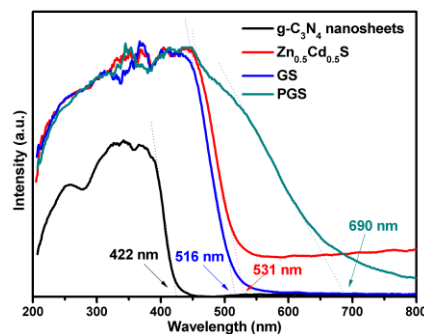

Fig. 4 UV-vis diffuse reflectance spectra of the as-obtained samples

The photocatalytic activity of the as-prepared samples was firstly evaluated by degradation of RhB pollutant under visible light irradiation. As shown in Fig. 5,we can find that negligible photodegradation is detected in the blank experiment in the absence of photocatalyst, indicating the high stability of RhB under this experimental condition. Therefore, we can rule out the effect of dye self-degradation on evaluating the photocatalytic ability. After visible light irradiation for 60min, only 15% and 50% of RhB can be removed by g-C_3N_4 nanosheets and $Zn_{0.5}Cd_{0.5}S$, respectively. However, under the same conditions, about 70% RhB can be degraded by $Zn_{0.5}Cd_{0.5}S$/g-C_3N_4, and nearly 97% of RhB can be removed by P-doped $Zn_{0.5}Cd_{0.5}S$/g-C_3N_4

within 30min. The obvious enhancement of photocatalytic activity may be attributed to the heterojunction formed between $Zn_{0.5}Cd_{0.5}S$ and g-C_3N_4 as well as the doping of P.
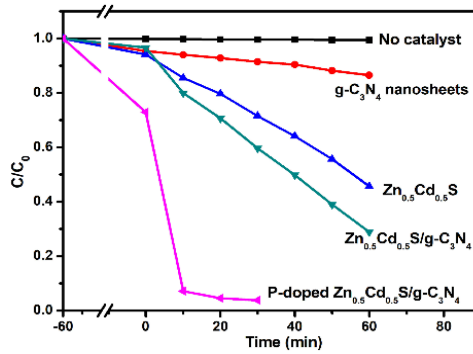

Fig. 5 The photocatalytic degradation of RhB by the as-prepared samples

Moreover, the photocatalytic activity for hydrogen generation with different samples from an aqueous solution containing 0.35 M Na_2S and 0.25 M Na_2SO_3 was evaluated under visible light irradiation. As can be seen from Fig. 6, the bare g-C_3N_4 NSs shows a very low photocatalytic activity towards water splitting and corresponding H_2 evolution rate is only 17.51 μmol g^{-1} h^{-1}. The low photocatalytic activity may be ascribed to the faster recombination of photo-generated holes and electrons due to the presence of interior defects created during the high-temperature preparation route [24]. Compared with bare g-C_3N_4 NSs, benefiting from the narrow bandgap and appropriate band edges, the pure $Zn_{0.5}Cd_{0.5}S$ NPs showed excellent photocatalytic activity with an H_2 production rate of 2174.36 μmol g^{-1} h^{-1}. Interestingly, both $Zn_{0.5}Cd_{0.5}S$/g-C_3N_4 and P-doped $Zn_{0.5}Cd_{0.5}S$/g-C_3N_4 exhibit improved photocatalytic activity for hydrogen generation. Their corresponding H_2 production rates (Fig. 6b) are determined to be 2660.82 μmol g^{-1} h^{-1} and 2880.83 μmol g^{-1} h^{-1} for $Zn_{0.5}Cd_{0.5}S$/g-C_3N_4 and P-doped $Zn_{0.5}Cd_{0.5}S$/g-C_3N_4, respectively. The significant enhancement of photocatalytic activities for photocatalytic water splitting could be ascribed to the synergetic effects of P doping and a close heterogeneous interface constructed between $Zn_{0.5}Cd_{0.5}S$ NPs and g-C_3N_4 NSs, which induce the faster separation of photo-generated electrons and holes, thus improving the photocatalytic performances.

(a) Photocatalytic hydrogen evolution　　　　(b) hydrogen production rate over different catalysts
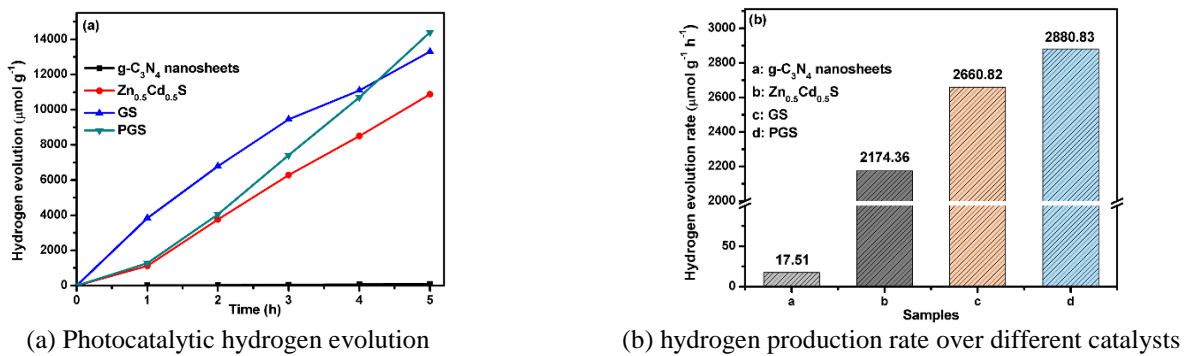
Fig. 6 Photocatalytic activity for hydrogen evolution

Generally, phase structure, morphology, light absorption intensity, the separation efficiency of photo-generated carrier charge pairs, etc. play important roles in deciding the photocatalytic activities [31-35]. However, the similar phase structure and morphology, the decreased light absorption indicate that these factors are not responsible for the significant enhancement of the photocatalytic performances. Fig. 7(a) shows the photocurrent response of the different samples with the exposure of discontinuous visible light. It can be clearly seen that PGS exhibits the highest photocurrent density among all the as-prepared samples, which implies that the photoinduced charge carriers can be separated efficiently after phosphorization. The efficient charge transfer was further confirmed by the Electrochemical Impedance Spectra (EIS) analysis as shown in Fig. 7(b). The EIS Nyquist plots reveal that the prepared PGS possesses a smaller semicircle in comparison with those of its counterparts, suggesting that the phosphorization process can enhance the separation and transfer efficiency of the charge carrier pairs.
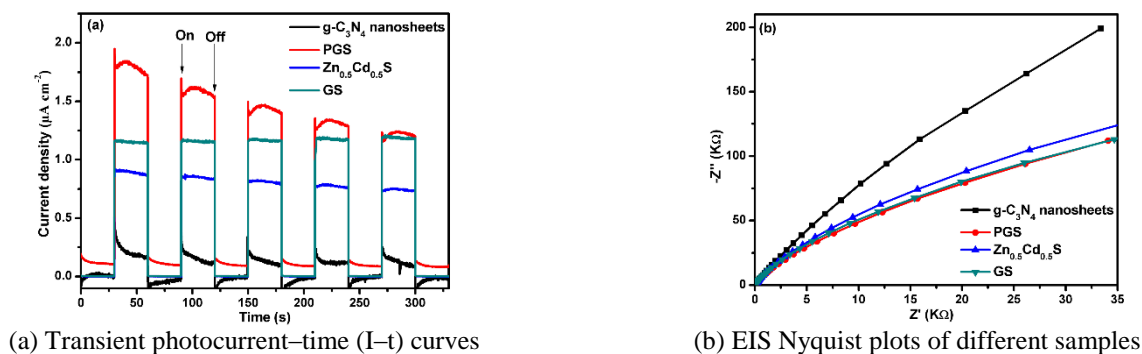
(a) Transient photocurrent–time (I–t) curves   (b) EIS Nyquist plots of different samples

Fig. 7 Photoelectrochemical tests of the as-prepared samples

4. Conclusions

In summary, the novel P-doped $Zn_{0.5}Cd_{0.5}S$/g-C_3N_4 heterostructured photocatalysts have been synthesized by in-situ deposition of $Zn_{0.5}Cd_{0.5}S$ nanoparticles on the surface of g-C_3N_4 nanosheets, followed by a phosphorization process. The as-prepared P-doped $Zn_{0.5}Cd_{0.5}S$/g-C_3N_4 composites in this work have been proved to be a better photocatalytic system than $Zn_{0.5}Cd_{0.5}S$/g-C_3N_4, and exhibit enhanced photocatalytic activity for RhB degradation and hydrogen evolution under visible light irradiation. The enhancement of photocatalytic activity, on the one hand, is mainly attributed to the unique property of g-C_3N_4 nanosheets, such as large surface areas and improved electron transportability. On the other hand, it also results from the synergetic effect of P doping and closes heterogeneous interface constructed between $Zn_{0.5}Cd_{0.5}S$ NPs and g-C_3N_4 NSs, which induce the faster separation of photo-generated electrons and holes. This work may provide a new possibility to further improve the performances of g-C_3N_4-based photocatalysts, and facilitates their applications in solar energy utilization and conversion.

Acknowledgement

Conflicts of Interest

The authors declare no conflict of interest.

References

[1] A. Fujishima and K. Honda, "Electrochemical photolysis of water at a semiconductor electrode," Nature, vol. 238, pp. 37-38, July 1972.

[2] D. Q. Zeng, P. Y. Wu, W. J. Ong, B. S. Tang, M. D. Wu, H. F. Zheng, Y. Z. Chen, and D. L. Peng, "Construction of network-like and flower-like 2H-MoSe2 nanostructures coupled with porous g-C3N4 for noble-metal-free photocatalytic H_2 evolution under visible light," Applied Catalysis B: Environment, vol. 233, pp. 26-34, October 2018.

[3] J. R. Ran, M. Jaroniec, and S. Z. Qiao, "Cocatalysts in semiconductor-based photocatalytic CO_2 reduction: achievements, challenges, and opportunities," Advanced Materials, vol. 30, pp. 1704649, February 2018.

[4] W. Chen, Z. C. He, G. B. Huang, C. L. Wu, W. F. Chen, and X. H. Liu, "Direct z-scheme 2D/2D $MnIn_2S_4$/g-C_3N_4 architectures with highly efficient photocatalytic activities towards treatment of pharmaceutical wastewater and hydrogen evolution," Chemical Engineering Journal, vol. 359, pp. 244-253, March 2019.

[5] X. Z. Chen, N. Li, Z. Z. Kong, W. J. Ong, and X. J. Zhao, "Photocatalytic fixation of nitrogen to ammonia: state-of-the-art advancements and future prospects," Materials Horizons, vol. 5, pp. 9-27, January 2018.

[6] R. B. We, Z. L. Huang, G. H. Gu, Z. Wang, L. X. Zeng, Y. B. Chen, and Z. Q. Liu, "Dual-cocatalysts decorated rimous CdS spheres advancing highly-efficient visible-light photocatalytic hydrogen production," Applied Catalysis B: Environment, vol. 231, pp. 101-107, September 2018.

[7]   S. Guo, Z. Deng, M. Li, B. Jiang, C. Tian, Q. Pan, and H. Fu, "Phosphorus-doped carbon nitride tubes with a layered micro-nanostructure for enhanced visible-light photocatalytic hydrogen evolution," Angewandte Chemie International Edition, vol. 55 pp. 1830-1834, December 2015.

[8]   L. Zhao, L. Zhang, H. Lin, Q. Nong, M. Cui, Y. Wu, and Y. He, "Fabrication and characterization of hollow $CdMoO_4$ coupled $g-C_3N_4$ heterojunction with enhanced photocatalytic activity," Journal of Hazardous Material, vol. 299, pp. 333-342, December 2015.

[9]   J. Zhang, J. G. Yu, M. Jaroniec, and J. R. Gong, "Noble metal-Free reduced graphene oxide-$Zn_xCd_{1-x}S$ nanocomposite with enhanced solar photocatalytic H2-production performance, " Nano Letter, vol. 12, pp. 4584-4589, August 2012.

[10] Q. J. Xiang, B. Cheng, and J. G. Yu, "Hierarchical porous CdS nanosheet-assembled flowers with enhanced visible-light photocatalytic H_2-production performance," Applied Catalysis B: Environment, vol. 138-139, pp. 299-303, July 2013.

[11] A. Kudo and Y. Miseki, "Heterogeneous photocatalyst materials for water splitting," Chemical Society Reviews, vol. 38, pp. 253-278, November 2008.

[12] W. Chen, G. R. Duan, T. Y. Liu, Z. M. Jia, X. H. Liu, S. M. Chen, and X. J. Yang, "Synthesis of homogeneous one-dimensional NixCd1-xS nanorods with enhanced visible-light response by ethanediamine-assisted decomposition of complex precursors," Journal of Material Science, vol. 50, pp. 3920-3928, June 2015.

[13] M. Liu, L. Zhang, X. He, B. Zhang, H. Song, S. Li, and W. You, "L-Cystine-assisted hydrothermal synthesis of $Mn_{1-x}Cd_xS$ solid solutions with hexagonal wurtzite structure for efficient photocatalytic hydrogen evolution under visible light irradiation," Journal of Material Chemistry A, vol. 2, pp. 4619-4626, January 2014.

[14] S. Xie, X. Lu, T. Zhai, J. Gan, W. Li, M. Xu, M. Yu, Y. M. Zhang, and Y. Tong, "Controllable synthesis of $Zn_xCd_{1-x}S@ZnO$ core@shell nanorods with enhanced photocatalytic activity," Langmuir, vol. 28, pp. 10558-10564, June 2012.

[15] R. Shi, H. F. Ye, F. Liang, Z. Wang, K. Li, Y. X. Weng, Z. S. Lin, W. F. Fu, C. M. Che, and Y. Chen, "Interstitial p-doped CdS with long-lived photogenerated electrons for photocatalytic water splitting without sacrificial agents," Advanced Materials, vol. 30, 1705941, December 2017.

[16] Z. Wu, G. Zhao, Y. Zhang, H. Tian, and D. Li, "Enhanced photocurrent responses and antiphotocorrosion performance of CdS hybrid derived from triple heterojunction," The Journal of Physical Chemistry C, vol. 116, pp. 12829-12835, May 2012.

[17] N. N. Hewa-Kasakarage, P. Z. El-Khoury, A. N. Tarnovsky, M. Kirsanova, I. Nemitz, A. Nemchinov, and M. Zamkov, "Ultrafast carrier dynamics in type II ZnSe/CdS/ZnSe Nanobarbells," ACS Nano, vol. 4, pp. 1837-1844, March 2010.

[18] Y. Tak, H. Kim, D. Lee, and K. Yong, "Type-II CdS nanoparticle-ZnO nanowire heterostructure arrays fabricated by a solution process: enhanced photocatalytic activity," Chemical Communication, pp. 4585-4587, August 2008.

[19] S. Liu, N. Zhang, Z. R. Tang, and Y. J. Xu, "Synthesis of one-dimensional $CdS@TiO_2$ core-shell nanocomposites photocatalyst for selective redox: the dual role of TiO2 shell," ACS Applied Materials & Interfaces, vol. 4, pp. 6378-6385, November 2012.

[20] H. Wang, L. Zhang, Z. Chen, J. Hu, S. Li, Z. Wang, J. Liu, and X. Wang, "Semiconductor heterojunction photocatalysts: design, construction, and photocatalytic performances," Chemical Society Reviews, vol. 43, pp. 5234-5244, May 2014.

[21] S. J. Moniz, S. A. Shevlin, D. J. Martin, Z. X. Guo, and J. Tang, "Visible-light driven heterojunction photocatalysts for water splitting: a critical review," Energy & Environmental Science, vol. 8, pp. 731-759, January 2015.

[22] M. C. Liu, D. W. Jing, Z. H. Zhou, and L. J. Guo, "Twin-induced one-dimensional homojunctions yield high quantum efficiency for solar hydrogen generation," Nature Communications, September 2013.

[23] J. G. Song, H. T. Zhao, R. R. Sun, X. Y. Li, and D. J. Sun, "An efficient hydrogen evolution catalyst composed of palladium phosphorous sulfide (PdP~0.33S~1.67) and twin nanocrystal $Zn_{0.5}Cd_{0.5}S$ solid solution with both homo and hetero-junctions," Energy & Environmental Science, vol. 10, pp. 225-235, November 2016.

[24] Q. Tay, P. Kanhere, C. F. Ng, S. Chen, S. Chakraborty, A. C. H. Huan, T. C. Sum, R. Ahuja, and Z. Chen, "Defect engineered $g-C_3N_4$ for efficient visible light photocatalytic hydrogen production," Chemistry of Materials, vol. 27, pp. 4930-4933, July 2015.

[25] Q. Lin, L. Li, S. Liang, M. Liu, J. Bi, and L. Wu, "Efficient synthesis of monolayer carbon nitride 2D nanosheets with tunable concentration and enhanced visible-light photocatalytic activities," Applied Catalysis B: Environment, vol. 163, pp. 135-142, February 2015.

[26] X. X. Wang, J. Chen, X. J. Guan, and L. J. Guo, "Enhanced efficiency and stability for visible light driven water splitting hydrogen production over $Cd_{0.5}Zn_{0.5}S/g-C_3N_4$ composite photocatalyst," International Journal of Hydrogen Energy, vol. 40, pp. 7546-7552, June 2015.

[27] H. Liu, Z. T. Jin, and Z. Z. Xu, "Hybridization of Cd0.2Zn0.8S with g-C3N4 nanosheets: a visible-light-driven photocatalyst for H2 evolution from water and degradation of organic pollutants," Dalton Transaction, vol.44, pp. 14368-14375, July 2015.

[28] J. Luo, X. Zhou, L. Ma, and X. Xu, "Enhancing visible-light photocatalytic activity of g-C_3N_4 by doping phosphorus and coupling with CeO_2 for the degradation of methyl orange under visible light irradiation," RSC Advances, vol. 5, pp. 68728-68735, August 2015.

[29] B. C. Zhu, P. F. Xia, W. K. Ho, and J. G. Yu, "Isoelectric point and adsorption activity of porous g-C_3N_4," Applied Surface Science, vol. 344, pp. 188-195, July 2015.

[30] J. Zhang, Y. Hu, X. Jiang, S. Chen, S. Meng, and X. Fu, "Design of a direct z-scheme photocatalyst: preparation and characterization of Bi_2O_3/g-C_3N_4 with high visible light activity," Journal of Hazardous Materials, vol. 280, pp. 713-722, September 2014.

[31] X. J. Bai, L. Wang, and Y. F. Zhu, "Visible photocatalytic activity enhancement of $ZnWO_4$ by graphene hybridization," ACS Catalysis, vol. 2, pp. 2769-2778, November 2012.

[32] N. Zhang, S. Q. Liu, X. Z. Fu, and Y. J. Xu, "Synthesis of M@TiO_2(M = Au, Pd, Pt) core-shell nanocomposites with tunable photoreactivity," The Journal of Physical Chemistry C, vol. 115, pp. 9136-9145, April 2011.

[33] H. X. Xong, T. Zhao, G. D. Zhou, R. F. Qian, T. Feng, and J. H. Pan, "Revisiting structural and photocatalytic properties of g-C_3N_4/TiO_2: is surface modification of TiO_2 by calcination with urea an effective route to solar photocatalyst ?" Catalysis Today, December 2018.

[34] R. F. Qian, H. X. Zong, J. Schneider, G. D. Zhou, T. Zhao, Y. L. Li, J. Yang, B. W. Bahnemann, and J. H. Pan, "Charge carrier trapping, recombination and transfer during TiO2 photocatalysis: an overview," Catalysis Today, October 2018.

[35] X. Z. Jiang, M. Manawan, T. Feng, R. F. Qian, T. Zhao, G. D. Zhou, F. T. Kong, Q. Wang, S. Y. Dai, and J. H. Pan, "Anatase and rutile in evonik aeroxide P25: heterojunctioned or individual nanoparticles?" vol. 300, pp. 12-17, February 2018.